Mg Alloying in SnTe Facilitates Valence Band Convergence and Optimizes Thermoelectric Properties

umesh waghmare

Cite this paper

Get the citation in MLA, APA, or Chicago styles

Related papers

Download a PDF Pack of the best related papers

Thermoelectric materials: Energy conversion between heat and electricity
Shetti Swamy

Thermoelectrics_from history a window to the future.pdf
Giacomo Cerretti

Thermoelectric properties of IV–VI-based heterostructures and superlattices
Horacio Alves

Article

Mg Alloying in SnTe Facilitates Valence Band Convergence and Optimizes Thermoelectric Properties

Ananya Banik,[†] U. Sandhya Shenoy,[‡] Shashwat Anand,[‡] Umesh V. Waghmare,[‡] and Kanishka Biswas*,[†]

[†]New Chemistry Unit and [‡]Theoretical Sciences Unit, Jawaharlal Nehru Centre for Advanced Scientific Research (JNCASR), Jakkur P.O., Bangalore 560064, India

S *Supporting Information*
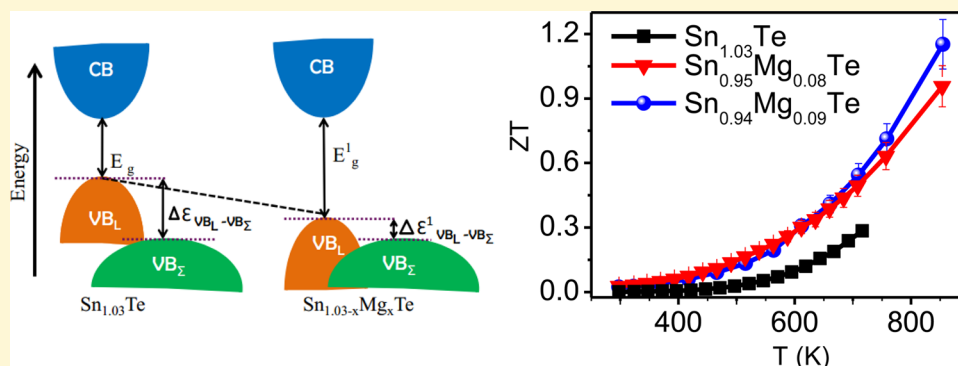
ABSTRACT: SnTe, a lead-free rock-salt analogue of PbTe, having valence band structure similar to PbTe, recently has attracted attention for thermoelectric heat to electricity generation. However, pristine SnTe is a poor thermoelectric material because of very high hole concentration resulting from intrinsic Sn vacancies, which give rise to low Seebeck coefficient and high electrical thermal conductivity. In this report, we show that SnTe can be optimized to be a high performance thermoelectric material for power generation by controlling the hole concentration and significantly improving the Seebeck coefficient. Mg (2−10 mol %) alloying in SnTe modulates its electronic band structure by increasing the band gap of SnTe and results in decrease in the energy separation between its light and heavy hole valence bands. Thus, solid solution alloying with Mg enhances the contribution of the heavy hole valence band, leading to significant improvement in the Seebeck coefficient in Mg alloyed SnTe, which in turn results in remarkable enhancement in power factor. Maximum thermoelectric figure of merit, *ZT*, of ∼1.2 is achieved at 860 K in the high quality crystalline ingot of *p*-type $Sn_{0.94}Mg_{0.09}Te$.

INTRODUCTION

A thermoelectric material can directly convert temperature difference to electrical voltage and, thus, can play an important role in generation of electrical energy from waste heat.[1−4] Materials in this field require a high value of dimensionless thermoelectric figure of merit, $ZT = \sigma S^2 T/(\kappa_{lat} + \kappa_{el})$, where σ is electrical conductivity, S is the Seebeck coefficient, κ_{lat} is lattice thermal conductivity, κ_{el} is electronic thermal conductivity, and T is temperature. Significant improvement in the ZT has been achieved through the reduction of κ_{lat} via phonon scattering by the solid solution point defects, second phase nanoprecipitates,[5−7] mesoscale grain boundaries,[6−8] and intrinsic bond anharmonicity.[9,10] Enhancement of Seebeck coefficient also resulted in high ZTs either through the formation of the resonance level in the electronic bands[11−13] or convergence of degenerate electronic band valleys by alloying and carrier engineering.[14−17]

Lead telluride (PbTe) and its alloys are considered to be some of the best thermoelectric materials for mid temperature power generation application.[1−3,5−7,11,14] Solid solution alloying and second phase nanostructuring with group-II (Mg, Ca,

Sr, and Ba) alkaline earth telluride have significant effect on thermoelectric property of PbTe.[5,6,16,18−20] Mention must be made that alloying of MgTe (band gap ∼3.5 eV) increases the band gap of PbTe, resulting in decrease in the energy separation between the light (*L* point) and heavy (Σ point) valence bands to accomplish more controllable band convergence with respect to temperature.[16,19,20] Thus, a significant enhancement in Seebeck coefficient was obtained. However, environmental concern about Pb limits its use in large scale thermoelectric applications. Tin telluride (SnTe), a homologue of PbTe, has the potential to be a good thermoelectric material due to its valence band (light hole and heavy hole valence bands) characteristic that is similar to PbTe.[21−23] SnTe has rarely been considered to be efficient thermoelectric material because of the inability to control its very high carrier concentration ($10^{20}−10^{21}$ cm$^{−3}$) which results in low S and high κ_{el}.[23] Intrinsic Sn vacancy is responsible for

high p-type carrier concentration in SnTe.[24] Recently, SnTe has been alloyed with other metal tellurides such as AgSbTe$_2$ to improve its thermoelectric performance.[25,26] Significant enhancement in the Seebeck coefficient of SnTe has been achieved due to the formation of the resonance level in the valence band through In doping, which resulted in a ZT of ~1.1 at 873 K.[13] Carrier concentration in the light hole valence band of SnTe was effectively tuned by iodine doping, which essentially tunes the thermoelectric properties of SnTe.[27]

In SnTe, valence band and conduction band edges are located at the L-point of the Brillouin zone, and the energy gap is ~0.15 eV at room temperature.[21] Interestingly, a heavy hole valence band (Σ band) lies ~0.35 eV below the light hole valence band (L band).[21−23] Earlier investigation based on temperature dependent Hall coefficient (R_H) measurement of SnTe suggested that the convergence of these two bands occurs at around 700 K.[28] Large energy separation between light and heavy hole valence bands restricts the contribution of heavy hole mass to the Seebeck coefficient. Enhancement in the Seebeck coefficient has been achieved by Cd or Hg alloying in SnTe, which decreases the energy separation between light and heavy hole valence band.[29] Solid solution alloying of SnTe with SnSe followed by In doping also improves the Seebeck coefficient due to resonance level formation in the valence band.[30] Alloying of SnTe (E_g ~ 0.15 eV) with MgTe, which is a wide band gap (E_g ~ 3.5 eV) semiconductor, may open up the band gap of SnTe, which can decrease the energy difference of the two valence bands of SnTe; thus, it will facilitate the convergence of the valence band valleys.

Here we present effects of Mg alloying on the electronic structure and the thermoelectric properties of SnTe which is synthesized by simple sealed tube melting reactions. We first suppress the excess hole concentration of SnTe by Sn self-compensation (Sn$_{1.03}$Te).[29a] Mg alloying in Sn$_{1.03}$Te samples increases the band gap, with direct evidence from the infrared diffuse reflectance spectroscopy and electronic structure calculations. Moreover, Mg alloying significantly tunes the electronic band structure of SnTe, which essentially decreases energy difference between the light hole and heavy hole valence bands, leading to an enhanced Seebeck coefficient. As a result, the p-type Sn$_{0.94}$Mg$_{0.09}$Te sample exhibits a maximum ZT of ~1.2 at ~860 K. These findings make SnTe-based materials an important contender for thermoelectric power generation and should stimulate further investigation and optimization.

■ EXPERIMENTAL AND THEORETICAL SECTION

Reagents. Tin (Alfa Aesar 99.99+ %), tellurium (Alfa Aesar 99.999+ %), and magnesium powder (Alfa Aesar 99.999+ %) were used for synthesis without further purification.

Synthesis. High quality crystalline ingots (~7 g) of Sn$_{1.03−x}$Mg$_x$Te (x = 0−0.12) were synthesized by mixing appropriate ratios of high-purity starting materials of Sn, Mg, and Te in a carbon coated quartz tube. Typically, to synthesize the Sn$_{0.94}$Mg$_{0.09}$Te sample, Sn (3.2359 g, 27.259 mmol), Mg (63.4 mg, 2.609 mmol), and Te (3.7003 g, 28.99 mmol) were used. The tubes were sealed under vacuum (10^{-5} Torr) and slowly heated to 450 °C over 12 h, then heated up to 900 °C in 5 h, soaked for 10 h, and cooled slowly to room temperature.

Powder X-ray Diffraction. Powder X-ray diffraction for all of the samples was recorded using a Cu Kα (λ = 1.5406 Å) radiation on a Bruker D8 diffractometer.

Band Gap Measurement. To estimate the optical energy difference between valence band and conduction band, optical diffuse reflectance measurement has been done with finely ground powder at room temperature using an FT-IR Bruker IFS 66 V/S spectrometer in a frequency range 4000−400 cm^{-1} with 2 cm^{-1} resolution and 50

scans. Absorption (α/Λ) data were calculated from reflectance data using Kubelka−Munk equations: $\alpha/\Lambda = (1 - R)^2/(2R)$, where R is the reflectance, and α and Λ are the absorption and scattering coefficients, respectively. The energy band gaps were derived from α/Λ vs E (eV) plots.

Electrical Transport. Electrical conductivity and Seebeck coefficients were measured simultaneously under He atmosphere from room temperature to 873 K on a ULVAC-RIKO ZEM-3 instrument system. The typical sample for measurement had a parallelepiped shape with the dimensions of ~2 × 2 × 8 mm^3. The longer direction coincides with the direction in which the thermal conductivity was measured. Heating and cooling cycles give repeatable electrical properties for a given sample (Figure S1, Supporting Information).

Hall Measurement. Carrier concentrations were determined using Hall coefficient measurements at room temperature with a PPMS system. Four-contact Hall-bar geometry was used for the measurement. At 300 K, we have estimated the carrier concentration, n, from the formula $n = 1/eR_H$, where e is the electronic charge and R_H is hall coefficient.

Thermal Conductivity. Thermal diffusivity, D, was directly measured in the range 300−873 K by using laser flash diffusivity method in a Netzsch LFA-457 (see the D vs T data in Figure S2, Supporting Information). Coins with ~8 mm diameter and ~2 mm thickness were used in all of the measurements. Temperature dependent heat capacity, C_p, was derived using standard sample (pyroceram) in LFA457, which is in good agreement with Dulong Petit C_p value (see Figure S3, Supporting Information). The total thermal conductivity, κ_{total}, was calculated using the formula $\kappa_{total} = DC_p\rho$, where ρ is the density of the sample, measured using the sample dimension and mass. The density of the pellets obtained was in the range ~96% of the theoretical density (Table S1, Supporting Information).

Computational Details. Density functional theoretical (DFT) electronic structure calculations of pristine SnTe and Mg alloyed SnTe were carried out using Quantum Expresso package.[31] Scalar relativistic norm conserving pseudo-potentials and a Generalized Gradient Approximation (GGA) to exchange-correlation energy with functional of Perdew, Burke, and Erzenhoff (PBE) were used to perform the DFT calculations.[32] The valence electrons of Sn, Te, and Mg ($5s^25p^2$, $5s^25p^4$, and $3s^2$ respectively) are included in calculations through the use of pseudo-potentials. SnTe is known to crystallize in rocksalt structure, while MgTe occurs in the zinc blend structure.[20] Mg substituted in the zinc blend site of SnTe was simulated with a tetragonal supercell ($\sqrt{2} \times \sqrt{2} \times 2$) containing 32 atoms. Plane wave basis for representing wave functions is terminated with energy cutoff of 40 Ry, and 14 × 14 × 10 mesh of k points was used in sampling Brillouin zone integrations. Electronic structure of Sn$_{16}$Te$_{16}$, Sn$_{15}$MgTe$_{16}$, and Sn$_{14}$Mg$_2$Te$_{16}$ with Mg atoms substituted for Sn atoms in SnTe is determined along high symmetry lines in the Brillouin zone, using a theoretical equilibrium lattice constant of 6.417 Å.

■ RESULTS AND DISCUSSION

Previously, SnTe was not considered to be a good thermoelectric material due to its very high carrier concentration (~10^{21}) resulting from intrinsic Sn vacancy.[23] Electron donor dopant such as iodine doping in SnTe has optimized the thermoelectric property by decreasing the carrier concentration.[27] Recently, Kanatzidis and co-workers have shown that self-compensation of Sn is an effective path for optimizing the thermoelectric performance of SnTe.[29] First, we have synthesized the self-compensated Sn$_{1.03}$Te sample, which shows significantly low hole concentration (~1.2 × 10^{20} cm^{-3}) compared to pristine SnTe (~4.5 × 10^{20} cm^{-3}). Further, the effect of Mg alloying on the thermoelectric property was investigated on self-compensated Sn$_{1.03}$Te sample.

Sn$_{1.03−x}$Mg$_x$Te (x = 0, 0.02, 0.03, 0.05, 0.07, 0.08, 0.09, 0.1) samples were synthesized by vacuum sealed tube melting
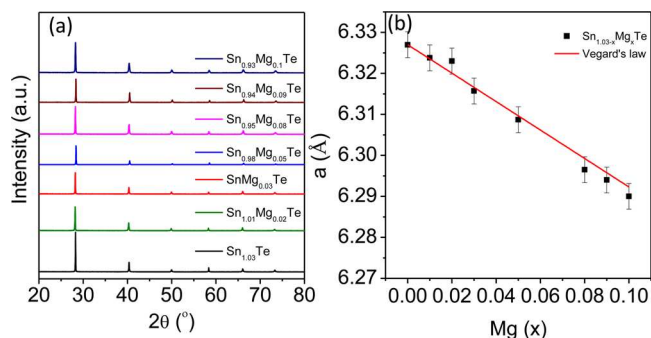
Figure 1. (a) Powder XRD patterns of $Sn_{1.03-x}Mg_xTe$ ($x = 0-0.1$) samples. (b) Lattice parameter (a) vs Mg concentration (x) in $Sn_{1.03-x}Mg_xTe$, and solid line indicates the Vegard's law for the solid solution.

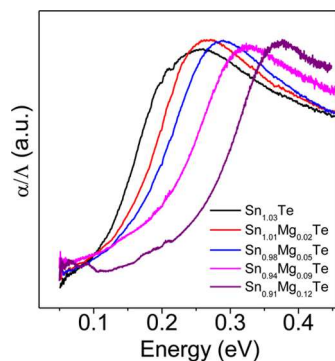**Figure 2.** Electronic absorption spectra of $Sn_{1.03-x}Mg_xTe$.

reaction and characterized by powder XRD. Figure 1a confirms formation of single phase nature within the detection limit of PXRD, and the patterns could be indexed on SnTe structure ($Fm\overline{3}m$ space group). As shown in Figure 1b, the lattice parameter decreases with increasing the Mg concentration, consistent with the smaller radius of Mg^{2+} (86 pm) compared to that of Sn^{2+} (93 pm). Linear decrease in the lattice parameter follows solid solution Vegard's law.

We were able to resolve the band gap of $Sn_{1.03-x}Mg_xTe$ ($x = 0-0.12$) by diffuse reflectance IR spectroscopy (Figure 2). With increasing Mg concentration up to 12 mol % the electronic absorption spectra of SnTe show a shift of absorption edge toward high energy. Generally, if MgTe ($E_g \sim 3.5$ eV) was dissolving in SnTe an increase in the band gap would be expected. The band gap derived from the plot shows an increase from ~0.11 eV to ~0.26 eV in going from 0% to 12% Mg in SnTe. This result is similar to that of MgTe alloyed with PbTe.[16] Increase in the band gap with Mg incorporation in SnTe is indicating reduction of the energy separation of light hole and heavy hole valence bands which will be discussed further in the later part of the paper.

Figure 3 shows electrical transport property of $Sn_{1.03-x}Mg_xTe$ ($x = 0-0.1$). For all samples electrical conductivity (σ) decreases with increase in temperature which is typical of a degenerate semiconductor (Figure 3a). The electrical conductivity decreases with increasing Mg concentration up to 9 mol %, especially at room temperature from 9650 S cm^{-1} to 3114 S cm^{-1} (Figure 3a). Typically, the room temperature σ of $Sn_{0.94}Te_{0.09}Te$ is to be 3114 S cm^{-1}, which decreases to 1015 S cm^{-1} at 856 K. The room temperature Hall coefficients, R_H, of all $Sn_{1.03-x}Mg_xTe$ ($x = 0-0.1$) samples are positive, which indicates the p-type conduction in this system. Interestingly, carrier concentration (n) at 300 K increases with increasing the Mg concentration up to 2 mol % and then almost remains flat with further increasing the Mg alloying up to 9 mol % (Figure 3b). Anomalous change in the carrier concentration with the increase of Mg is difficult to explain, but similar behavior has been observed recently in In doped SnTe[13] and $SnTe_{1-x}Se_x$[30] and Cd alloyed SnTe.[29a] A recent report also shows the anomalous change in the carrier concentration in Hg doped SnTe.[29b] Although Mg, Cd, and Hg are supposed to be isovalent with Sn, Cd appears to act as electron donor, whereas Mg and Hg act as electron acceptors. The effect of different doping on the carrier concentration of SnTe is not very clear yet. Room temperature carrier mobility (μ) decreases with Mg concentration in $Sn_{1.03-x}Mg_xTe$ (Figure 3c), which is probably due to the impurity scattering and the increased effective mass of holes caused by modification of electronic band structure.[13,30] Decrease in room temperature σ value with the increase in Mg doping concentration is due to the decrease in μ.

Figure 4a represents temperature dependence of the Seebeck coefficient (S) of $Sn_{1.03-x}Mg_xTe$ samples. A positive value of S indicates p-type conduction which supports the Hall coefficient
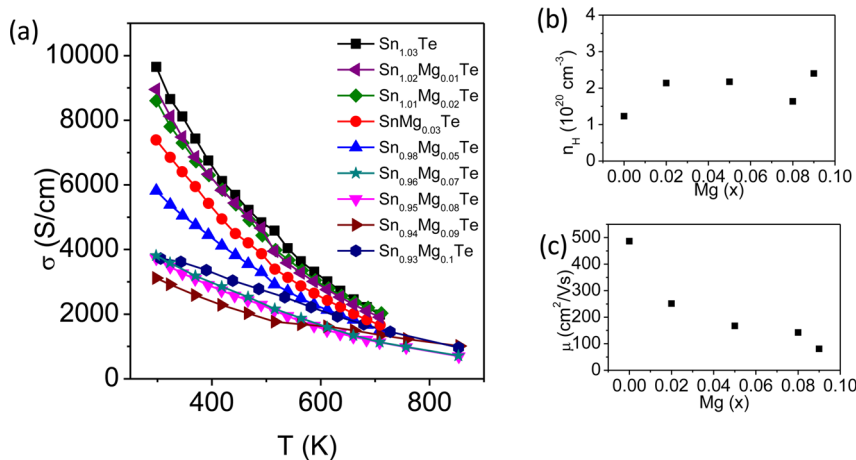

Figure 3. (a) Temperature dependent electrical conductivity (σ) of $Sn_{1.03-x}Mg_xTe$ samples. (b) Carrier concentration (n) and (c) carrier mobility (μ) at room temperature with respect to Mg alloying concentration (x) in $Sn_{1.03-x}Mg_xTe$.
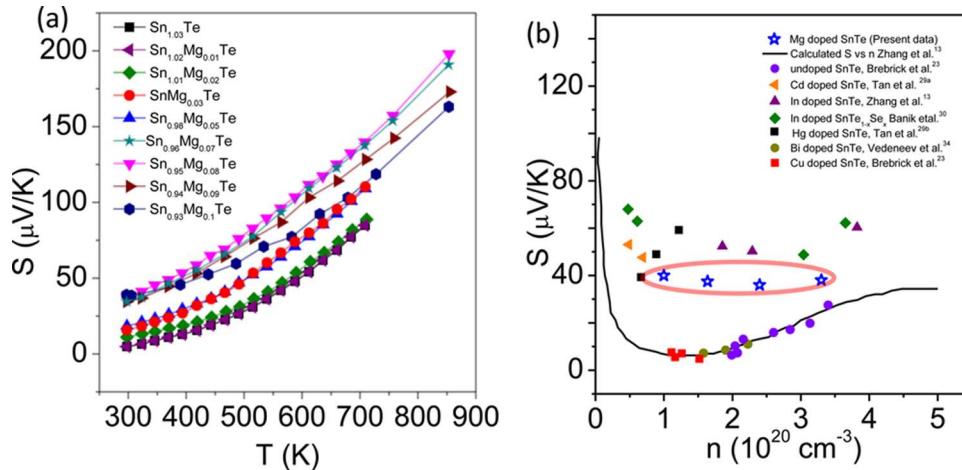
Figure 4. (a) Temperature dependent Seebeck coefficient (S) of $Sn_{1.03-x}Mg_xTe$ samples; (b) room temperature S vs n plot of the present $Sn_{1.03-x}Mg_xTe$ samples. For comparison, previously reported S vs n experimental data of undoped SnTe,[23] Cd doped SnTe,[29a] In doped SnTe,[13] In doped $SnTe_{0.85}Se_{0.15}$,[30] Hg doped SnTe,[29b] Bi doped SnTe,[34] Cu-doped SnTe,[23] and theoretical Pisarenko curve based on VBM model[13] are given in (b).

Table 1. Room Temperature Carrier Concentration (n_H) and Effective Mass (m^*) of $Sn_{1.03-x}Mg_xTe$ Samples Where m_e Is Mass of Electron

composition	n (10^{20} cm^{-3})	m^* (m_e)
$Sn_{1.03}Te$	1.2	0.16
$Sn_{1.01}Mg_{0.02}Te$	2.1	0.24
$Sn_{0.98}Mg_{0.05}Te$	2.2	0.33
$Sn_{0.96}Mg_{0.07}Te$	3.3	0.91
$Sn_{0.95}Mg_{0.08}Te$	1.6	0.55
$Sn_{0.94}Mg_{0.09}Te$	2.4	0.69
$Sn_{0.93}Mg_{0.1}Te$	1.0	0.43

measurement. Significant enhancement in S has been achieved by Mg alloying in SnTe, both at room temperature and high temperatures. Typically, the room temperature S value measured for $Sn_{0.95}Mg_{0.08}Te$ was ~38 μV K^{-1}, which linearly increases to ~200 μV K^{-1} at 856 K. High temperature (~856 K) S values for $Sn_{0.96}Mg_{0.07}Te$, $Sn_{0.95}Mg_{0.08}Te$, $Sn_{0.94}Mg_{0.09}Te$, and $Sn_{0.93}Mg_{0.1}Te$ are 192, 200, 175, and 165 μV K^{-1}, respectively. We have estimated effective mass (m^*) of $Sn_{1.03-x}Mg_xTe$ samples using the measured S and Hall carrier concentration (n) at room temperature.[17,33] Although an accurate calculation of m^* requires consideration of the nonparabolic band and multiple band model, present calculation of m^* considers only a single parabolic band for simplicity.[17,33] Increase in effective mass from ~0.16 m_e to ~0.69 m_e with increasing the Mg concentration from 0 to 9 mol % is observed (Table 1), which is resulting probably due to the increasing contribution of the heavy hole valence band of SnTe.

In Figure 4b, we compare the present room temperature S vs n data of $Sn_{1.03-x}Mg_xTe$ samples with previously reported experimental data on In doped SnTe,[13] In doped $SnTe_{1-x}Se_x$,[30] Cd alloyed SnTe,[29a] Hg alloyed SnTe,[29b] Bi doped SnTe,[34] and Cu doped SnTe[23] and also with the earlier reported theoretical S vs n curves by Zhang et al.[13] Theoretical Pisarenko (S vs n) curves at room temperature have been calculated earlier by considering the contribution of both the light hole valence band (L point) and heavy hole valence band (Σ point) of SnTe.[13] This model uses a light hole band effective mass of ~0.168 m_e, a heavy hole band effective mass of ~1.92 m_e, and an energy gap between two valence bands of 0.35 eV, respectively. Indium

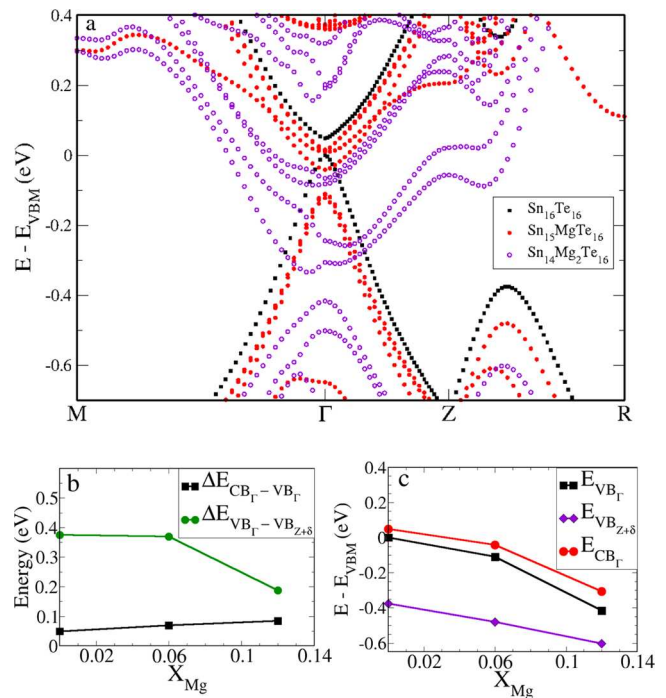**Figure 5.** (a) Electronic band structures of $Sn_{16}Te_{16}$, $Sn_{15}MgTe_{16}$, and $Sn_{14}Mg_2Te_{16}$ supercell as a function of wave vector in the supercell brillouin zone. The energies shown are relative to the valence band maximum of $Sn_{16}Te_{16}$. The band gap appears at the Γ point and heavy hole band at $Z + \delta$ in the ($\sqrt{2} \times \sqrt{2} \times 2$) tetragonal supercell. The VBM and CBM occurring at L point in the rocksalt cell of SnTe fold on to the Γ point, and the heavy hole valence band appearing along Σ folds on to $Z + \delta$ in the case of present 32 atom ($\sqrt{2} \times \sqrt{2} \times 2$) tetragonal supercell. (b) Band gap ($\Delta E_{CB\Gamma-VB\Gamma}$) and energy difference ($\Delta E_{VB\Gamma-VB(Z+\delta)}$) between two valence bands as a function of concentration of Mg in SnTe. (c) The energies of light hole valence band (Γ), heavy hole valence band ($Z + \delta$), and conduction band (Γ) as a function of concentration of Mg in SnTe.

and Cd/Hg alloyed SnTe samples show much higher Seebeck coefficient than that of the theoretical Pisarenko curve due to the effect of resonance level formation[13,30] and valence band convergence,[29] respectively. We observe that $Sn_{1.03-x}Mg_xTe$

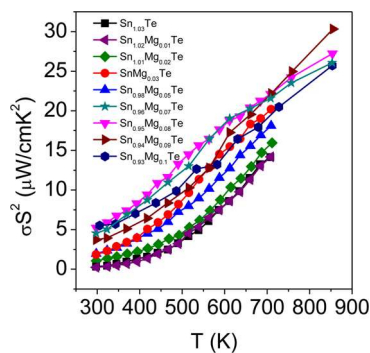**Figure 6.** Temperature dependence of the power factor (σS^2) of $Sn_{1.03-x}Mg_xTe$ samples.

Figure 8. Temperature dependence of thermoelectric figure of merit (ZT) of $Sn_{1.03-x}Mg_xTe$ samples with 10% error bar.

samples also show significantly large Seebeck coefficients compared to that of the Pisarenko curve (Figure 4b).

In order to understand the origin of enhancement in Seebeck coefficient we have performed DFT calculation of electronic structure of SnTe and Mg-alloyed SnTe (see in Figure 5a). For $Sn_{16}Te_{16}$, $Sn_{15}MgTe_{16}$ (6 mol % Mg alloyed), and $Sn_{14}Mg_2Te_{16}$ (12 mol % Mg alloyed) systems, the principal valence band (light hole) maximum (VBM) and conduction band minima (CBM) occur at the Γ point and the heavy hole band is at $Z + \delta$ along the $Z \rightarrow R$ direction. The VBM and CBM occurring at the L point in the Brillouin zone of the cubic cell of SnTe folds onto the Γ point, and the heavy hole valence band appearing along Σ folds on to $Z + \delta$ in the Brillouin zone of the 32 atom ($\sqrt{2} \times \sqrt{2} \times 2$) tetragonal supercell. The band gap of SnTe increases with increasing Mg alloying, consistent with the trend of the experimental band gap measured by diffuse reflectance spectroscopy. The band gap of ~0.049 eV was obtained in the case of SnTe, which is in good agreement with previous calculation which does not consider the spin orbit coupling.[29a] The band gap of 0.049 eV of $Sn_{16}Te_{16}$ at the Γ point increases to 0.069 and 0.084 eV with substitution of 6 mol % and 12 mol % Mg for Sn atoms, respectively (Figure 5b). This is due to the larger decrease in the energy of the valence band in comparison with the conduction band at the Γ point leading to opening of the band gap (Figure 5c).

Significant decrease in the energy separation between the light and the heavy valence band of SnTe is achieved with Mg alloying. The energy separation between the light hole and the
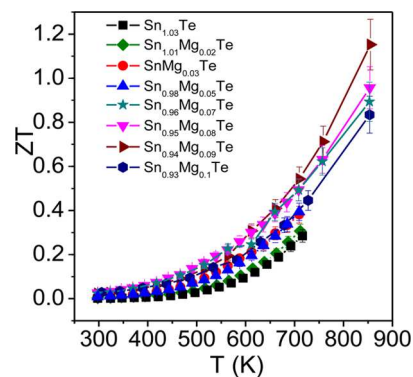
heavy hole valence band decreases from 0.375 eV for pristine SnTe to 0.18 eV for the 12 mol % Mg alloyed SnTe sample (Figure 5c). Thus, incorporation of Mg in the SnTe leads to increase in the valence band degeneracy. Such valence band convergence is expected to result in enhancement of the Seebeck coefficient due to contribution from both the bands, as there is an asymmetric increase in the density of states near the Fermi energy. Similar band modifications have been found in Cd/Hg alloyed SnTe[29] and Cd and Mg alloyed PbTe.[16,19]

Figure 6 represents temperature dependent power factor (σS^2) data of $Sn_{1.03-x}Mg_xTe$ ($x = 0-0.1$) samples. Benefiting from the significant enhancement in Seebeck coefficient both in low and high temperatures, Mg alloyed $Sn_{1.03}Te$ samples have much higher power factors than the undoped $Sn_{1.03}Te$ sample, with maximum values reaching to ~30.3 $\mu W\ cm^{-1}\ K^{-2}$ (Figure 6). The maximum power factor values obtained in the present $Sn_{1.03-x}Mg_xTe$ ingot samples are indeed higher than those of previously reported spark plasma sintered In and Cd/Hg alloyed SnTe samples.[13,29] Typically, at room temperature, the σS^2 value for $Sn_{0.94}Mg_{0.09}Te$ is to be ~3.5 $\mu W\ cm^{-1}\ K^{-2}$ which rises to ~30.3 $\mu W\ cm^{-1}\ K^{-2}$ at ~856 K.

In Figure 7, we present the temperature dependent total thermal conductivity (κ_{total}) and lattice thermal conductivity (κ_{lat}) of $Sn_{1.03-x}Mg_xTe$ ($x = 0-0.1$) samples. The κ_{lat} was obtained after subtracting the electronic part, κ_{el}, from the κ_{total}. The electronic thermal conductivities, $\kappa_{el} = L\sigma T$, were extracted based on fitting of the respective Seebeck values that estimate

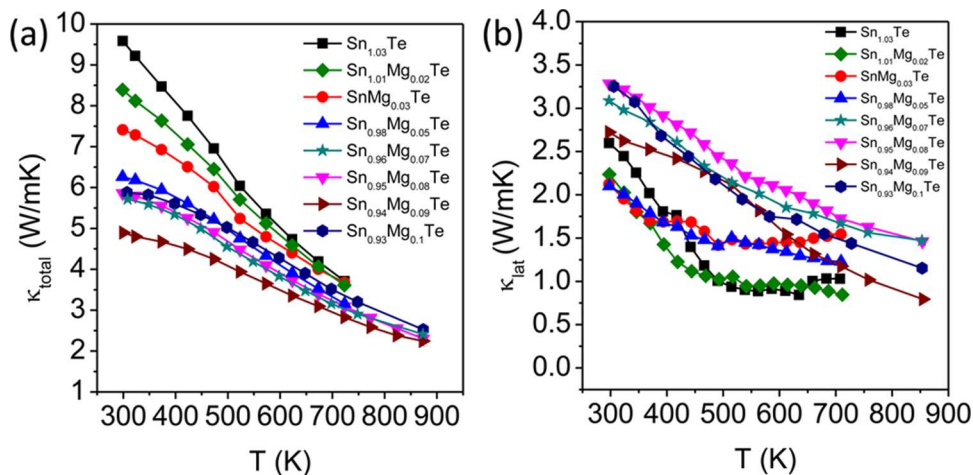**Figure 7.** Temperature-dependent (a) total thermal conductivity (κ_{total}) and (b) lattice thermal conductivity (κ_{lat}) of $Sn_{1.03-x}Mg_xTe$ samples.

the reduced chemical potential from which the Lorenz number, L, can be obtained as explained in detail previously (Figure S4, Supporting Information).[16,17] Mg alloying in $Sn_{1.03}Te$ optimizes the temperature dependent κ_{total} by controlling the κ_{el} (Figure S5, Supporting Information). With increasing the Mg concentration κ_{total} decreases due to the systematic decrease in κ_{el}. Typically, the room temperature κ_{total} value measured for $Sn_{0.94}Mg_{0.09}Te$ is ~4.9 W m^{-1} K^{-1} which decreases to ~2.2 W m^{-1} K^{-1} at 873 K. Interestingly we have not observed any systematic trend for κ_{lat} with Mg concentration in $Sn_{1.03}Te$. Typically, the room temperature κ_{lat} value measured for $Sn_{0.94}Mg_{0.09}Te$ is ~2.7 W m^{-1} K^{-1} which decreases to ~0.78 W m^{-1} K^{-1} at 856 K, which is slightly higher compared to Cd/ Hg alloyed SnTe samples.[29]

In Figure 8, we present temperature dependent ZT of $Sn_{1.03-x}Mg_xTe$ ($x = 0-0.10$) samples. The highest ZT value of ~1.2 at 856 K was achieved for $Sn_{0.94}Mg_{0.09}Te$, which is significantly higher compared to the undoped $Sn_{1.03}Te$ sample. The highest ZT obtained in the present crystalline ingot sample synthesized by simple melting reaction is indeed comparable to previously reported maximum ZT of spark plasma sintered Cd alloyed ($ZT \sim 1.3$ at 873 K),[29a] Hg alloyed ($ZT \sim 1.35$ at 910 K),[29b] and In doped ($ZT \sim 1.1$ at 873 K) SnTe samples.[13] Average ZT of $Sn_{0.94}Mg_{0.09}Te$ is ~0.6 by considering the hot and cold ends to 860 and 300 K, respectively, which is indeed comparable to the previously reported In doped SnTe ($ZT_{ave} \sim 0.6$) and Cd-doped SnTe ($ZT_{ave} \sim 0.65$).

CONCLUSIONS

p-type SnTe can be optimized to be a good thermoelectric material for power generation by controlling the hole concentration and improving the Seebeck coefficient. Mg alloying increases the band gap of $Sn_{1.03-x}Mg_xTe$ ($x = 0-0.9$) samples, which resulted in a decrease in the energy separation between two valence bands (light and heavy holes) of SnTe. Thus, effective convergence of the valence bands giving rise to significant enhancement in the Seebeck coefficient resulted in a remarkable increase in the power factor of $Sn_{1.03-x}Mg_xTe$ ($x = 0-0.1$). This type of band engineering is a crucial finding of this work and is important in achieving a high figure of merit of ~1.2 at 856 K for the p-type $Sn_{0.94}Mg_{0.09}Te$ sample. Present research suggests that SnTe-based materials are important candidates for thermoelectric power generation and provide the promise to act as alternative of lead chalcogenides in near future.

ASSOCIATED CONTENT

Ⓢ Supporting Information

Heating–cooling cycle data for a typical sample, temperature dependent diffusivity (D), heat capacity (C_p), Lorenz number (L), electronic thermal conductivity (κ_{el}) of $Sn_{1.03-x}Mg_xTe$, and electronic band structure of $Sn_{16}Te_{16}$, $Sn_{15}MgTe_{16}$, and $Sn_{14}Mg_2Te_{16}$. This material is available free of charge via the Internet at http://pubs.acs.org.

AUTHOR INFORMATION

Corresponding Author

*E-mail: kanishka@jncasr.ac.in.

Notes

The authors declare no competing financial interest.

REFERENCES

(1) Sootsman, J.; Chung, D. Y.; Kanatzidis, M. G. Angew. Chem., Int. Ed. 2009, 48, 8616.
(2) Zhao, L. D.; Dravid, V. P.; Kanatzidis, M. G. Energy Environ. Sci. 2014, 7, 251.
(3) Snyder, G. J.; Toberer, E. S. Nat. Mater. 2008, 7, 105.
(4) (a) Zebarjadi, M.; Esfarjani, K.; Dresselhaus, M. S.; Ren, Z. F.; Chen, G. Energy Environ. Sci. 2012, 5, 5147. (b) Zhang, Y.; Stucky, G. D. Chem. Mater. 2014, 26, 837. (c) Gaultois, M. W.; Sparks, T. D.; Borg, C. K. H.; Seshadri, R.; Bonificio, W. D.; Clarke, D. R. Chem. Mater. 2013, 25, 2911.
(5) Biswas, K.; He, J.; Zhang, Q.; Wang, G.; Uher, C.; Dravid, V. P.; Kanatzidis, M. G. Nat. Chem. 2011, 3, 160.
(6) Biswas, K.; He, J.; Blum, I. D.; Wu, C. I.; Hogan, T. P.; Seidman, D. N.; Dravid, V. P.; Kanatzidis, M. G. Nature 2012, 489, 414.
(7) Zhao, L. D.; Hao, S.; Lo, S. H.; Wu, C. I.; Zhou, X.; Lee, Y.; Li, H.; Biswas, K.; Hogan, T. P.; Uher, C.; Wolverton, C.; Dravid, V. P.; Kanatzidis, M. G. J. Am. Chem. Soc. 2013, 135, 7364.
(8) Poudel, B.; Hao, Q.; Ma, Y.; Lan, Y.; Minnich, A.; Yu, B.; Yan, X.; Wang, D.; Muto, A.; Vashaee, D.; Chen, X.; Liu, J.; Dresselhaus, M. S.; Chen, G.; Ren, Z. Science 2008, 320, 634.
(9) Zhao, L. D.; Lo, S. H.; Zhang, Y.; Sun, H.; Tan, G.; Uher, C.; Wolverton, C.; Dravid, V. P.; Kanatzidis, M. G. Nature 2014, 508, 373.
(10) Morelli, D. T.; Jovovic, V.; Heremans, J. P. Phys. Rev. Lett. 2008, 101, 035901.
(11) Heremans, J. P.; Jovovic, V.; Toberer, E. S.; Saramat, A.; Kurosaki, K.; Charoenphakdee, A.; Yamanaka, S.; Snyder, G. J. Science 2008, 321, 554.
(12) Ahmad, S.; Hoang, K.; Mahanti, S. D. Phys. Rev. Lett. 2006, 96, 56403.
(13) Zhang, Q.; Liao, B.; Lan, Y.; Lukas, K.; Liu, W.; Esfarjani, K.; Opeil, C.; Broido, D.; Chen, G.; Ren, Z. Proc. Natl. Acad. Sci. U.S.A. 2013, 110, 13261.
(14) Pei, Y.; Shi, X.; LaLonde, A.; Wang, H.; Chen, L.; Snyder, G. J. Nature 2011, 473, 66.
(15) Liu, W.; Tan, X.; Yin, K.; Liu, H.; Tang, X.; Shi, J.; Zhang, Q.; Uher, C. Phys. Rev. Lett. 2012, 108, 166601.
(16) Zhao, L. D.; Wu, H. J.; Hao, S. Q.; Wu, C. I.; Zhou, X. Y.; Biswas, K.; He, J. Q.; Hogan, T. P.; Uher, C.; Wolverton, C.; Dravid, V. P.; Kanatzidis, M. G. Energy Environ. Sci. 2013, 6, 3346.
(17) Guin, S. N.; Chatterjee, A.; Negi, D. S.; Datta, R.; Biswas, K. Energy Environ. Sci. 2013, 6, 2603.
(18) (a) Biswas, K.; He, J.; Wang, G.; Lo, S. H.; Uher, C.; Dravid, V. P.; Kanatzidis, M. G. Energy Environ. Sci. 2011, 4, 4675. (b) Lo, S. H.; He, J.; Biswas, K.; Kanatzidis, M. G.; Dravid, V. P. Adv. Funct. Mater. 2012, 22, 5175.
(19) Pei, Y. Z.; LaLonde, A. D.; Heinz, N. A.; Shi, X. Y.; Iwanaga, S.; Wang, H.; Chen, L.; Snyder, G. J. Adv. Mater. 2011, 23, 5674.
(20) Ohta, M.; Biswas, K.; Lo, S. H.; He, J.; Chung, D. Y.; Dravid, V. P.; Kanatzidis, M. G. Adv. Energy Mater. 2012, 2, 1117.
(21) Rogers, L. M. J. Phys. D: Appl. Phys. 1968, 1, 845.
(22) Efimova, B. A.; Kaidanov, V. I.; Moizhes, B. Y.; Chernik, I. A. Sov. Phys. - Solid State 1966, 7, 2032.
(23) Brebrick, R. F.; Strauss, A. J. Phys. Rev. 1963, 131, 104.
(24) Brebrick, R. F. J. Phys. Chem. Solids 1963, 24, 27.
(25) Han, M. K.; Androulakis, J.; Kim, S. J.; Kanatzidis, M. G. Adv. Energy Mater. 2012, 2, 157.
(26) Chen, Y.; Nielsen, M. D.; Gao, Y. B.; Zhu, T. J.; Zhao, X.; Heremans, J. P. Adv. Energy Mater. 2012, 2, 58.
(27) Zhou, M.; Gibbs, Z. M.; Wang, H.; Han, Y.; Xin, C.; Li, L.; Snyder, G. J. Phys. Chem. Chem. Phys. 2014, 16, 20741.
(28) Andreev, A. A. Sov. Phys. - Solid State 1967, 9, 1232.

(29) (a) Tan, G.; Zhao, L. D.; Shi, F.; Doak, J. W.; Lo, S.-H.; Sun, H.; Wolverton, C.; Dravid, V. P.; Uher, C.; Kanatzidis, M. G. *J. Am. Chem. Soc.* **2014**, *136*, 7006. (b) Tan, G.; Shi, F.; Doak, J. W.; Sun, H.; Zhao, L. D.; Wang, P.; Uher, C.; Wolverton, C.; Dravid, V. P.; Kanatzidis, M. G. *Energy Environ. Sci.* **2014**, *8*, 267.

(30) Banik, A.; Biswas, K. *J. Mater. Chem. A* **2014**, *2*, 9602.

(31) Giannozzi, P.; Baroni, S.; Bonini, N.; Calandra, M.; Car, R.; Cavazzoni, C.; Ceresoli, D.; Chiarotti, G. L.; Cococcioni, M.; DaboI; Corso, A. D.; Gironkoli, S. de; Fabris, S.; Fratesi, G.; Gebauer, R.; Gerstmann, U.; Gougoussis, C.; Kokalj, A.; Lazzeri, M.; Martin-Samos, L.; Marzari, N.; Mauri, F.; Mazzarello, R.; Paolini, S.; Pasquarello, A.; Paulatto, L.; Sbraccia, C.; Scandolo, S.; Sclauzero, G.; Seitsonen, A. P.; Smogunov, A.; Umari, P.; Wentzcovitch, R. M. *J. Phys.: Condens. Matter* **2009**, *21*, 395502.

(32) Perdew, J. P.; Burke, K.; Ernzerhof, M. *Phys. Rev. Lett.* **1996**, *77*, 3865.

(33) Guin, S. N.; Negi, D. S.; Datta, R.; Biswas, K. *J. Mater. Chem. A* **2014**, *2*, 4324.

(34) Vedeneev, V. P.; Krivoruchko, S. P.; Sabo, E. P. *Semiconductors* **1998**, *32*, 241.